


Dimensionally driven crossover from semimetal to direct semiconductor in layered SbAs

Shiqiang Hao ¹, Jiangang He,¹ Vinayak P. Dravid,¹ Mercuri G. Kanatzidis,² and Christopher Wolverton¹¹*Department of Materials Science and Engineering, Northwestern University, Evanston, Illinois 60208, USA*²*Department of Chemistry, Northwestern University, Evanston, Illinois 60201, USA*

(Received 20 August 2019; published 17 October 2019)

Two-dimensional (2D) materials have attracted a great deal of attention because they exhibit intriguing physical and chemical properties with great potential applications in electronic and optoelectronic devices, and even energy conversion. Due to the high anisotropy and unique crystal structure of layered materials, the properties can be effectively tuned by simply reducing dimensions to 2D. In this work, a unique 2D semiconductor, namely, monolayered SbAs, with high stability and indirect band gap, is predicted on the basis of first-principles calculations together with cluster expansion and Monte Carlo simulations. Interestingly, although the bulk antimony arsenide compound SbAs is known to exhibit semimetallic behavior, our calculations find that it is transformed into a direct semiconductor with a band gap of 1.28 eV when thinned down to a single atomic layer. The monolayer with antisite defects is transformed from indirect into a direct band-gap semiconductor. Such dramatic changes in the electronic structure could pave the way for SbAs to play a role in electronic device applications. Moreover, we find that the interlayer interactions in SbAs lead to a higher exfoliation energy than typical transition metal dichalcogenides such as MoS₂, and hence we suggest that chemical deposition methods might be better than mechanical exfoliation methods for obtaining monolayer samples.

DOI: [10.1103/PhysRevMaterials.3.106002](https://doi.org/10.1103/PhysRevMaterials.3.106002)

I. INTRODUCTION

It is known that crystalline As and Sb have a rhombohedral structure, which has been interpreted as resulting from a Peierls distortion from an ideal simple cubic structure [1]. Analogous to a Jahn-Teller distortion to characterize the instability of a molecule, the Peierls distortion is driven by an electronic instability for certain solids, where the partially filled bands have an innate tendency to lower their electronic energy by opening a band gap at the Fermi level [2]. The structural modulation driven by the Peierls distortion is usually accompanied by a metal-to-semiconductor or metal-to-insulator transition. This is due to the fact that the modulation diminishes the density of states at the Fermi level. However, the band structures of crystalline As and Sb have a weak overlap between valence and conduction bands leading to a small number of carriers compared to metals [3]. This peculiarity, namely, the semimetallic state with a nearly equal concentration of electrons and holes, results in an enhancement of many transport properties and is thus a fascinating research arena [3].

Combining alloying isostructural materials is a traditional way to tune material properties through the formation of intermediate compounds [4,5]. Since the band overlap in semimetals is so delicate, alloying As and Sb represents a very promising routine for tuning electronic properties. The phase diagram in the As-Sb system has been reported to show a complete solubility in the solid solution below the solidus curve, which shows a minimum transition temperature at 605 °C [6]. Later experiments confirmed both the high-temperature (>605 °C) features and the low-temperature (~ 300 °C $< T < 605$ °C) features, namely, a homogenization reaction which leads to the formation of a complete solid

solution [7]. However, Ohyama's study of the thermal conductivity for a series of Sb_{1-x}As_x alloys at 298 K found that the lattice thermal conductivity around $x = 0.5$ was anomalously higher than other compositions. It was suggested that the increase in lattice thermal conductivity is due to the possible existence of an ordered SbAs compound. However, this work lacked any structural characterization to substantiate this claim [8]. More recent, single-crystal and synchrotron x-ray diffraction experiments have shown that antimony arsenide (SbAs) is a stable compound displaying chemical ordering of Sb and As in the same rhombohedral structure as the elements with an order-disorder transition around 550 K [9]. Similar to the elements As and Sb, the SbAs is also a semimetal with a strong tendency to ordering in the Sb and As atoms, as confirmed previously by crystallographic studies and the transport and infrared reflectivity measurements along with first-principles calculations [9].

Though there are many allotropes for bulk As and Sb, the most stable gray arsenic (α -As, space group $R-3m$) and antimony are isostructural in a double-layered configuration consisting of many interlocked six-membered rings. The relatively weak bonding between layers suggests the possibility of fabricating monolayers as two-dimensional (2D) materials. Thinning down layered semiconductor bulk materials to a few- or single-layer 2D limits has recently become a powerful approach for tuning band gaps for electronic and optical applications [10,11]. A well known example is the highly anisotropic MoS₂ which exhibits a crossover from an indirect to a direct gap semiconductor when going from the bulk to its monolayer limit [12,13]. The band structure crossover to a direct gap accounts for a great enhancement of the observed photoluminescence in monolayer MoS₂ [14]. The dramatic evolution of the electronic structure stems from the spatial

distribution of d -electron orbitals of MoS₂ and strong inter-layer coupling between Mo and S electronic orbitals, which depend sensitively on layer thickness [14]. Tuning the band gap may also be used to optimize the material's use as a photocatalyst and for photovoltaic applications.

In this work, we clarify the phase stability of the As-Sb system, by constructing the temperature-composition phase diagram of Sb-As. We confirm the stable ordered structure of SbAs by means of a combination of density functional theory (DFT) calculations, cluster expansion (CE), and semi-grand canonical Monte Carlo (GCMC) simulations. With a set of well converged cluster interactions, we compute the partial long-range order in this compound, which is directly related to the percentage of antisite defects as a function of temperature, and find good agreement with experimental observations. From the stable ordered structure of SbAs, we predict that the electronic structure transitions from a semimetal to a semiconductor as the dimensionality of the material is reduced from bulk to monolayer. The 2D SbAs monolayer is an indirect semiconductor with a band gap of 1.28 eV, while the incorporation of antisites into monolayer SbAs results in a further transformation to a direct band semiconductor. Similar to 2D MoS₂, our results imply that aside from promising electronic and optoelectronic properties, these two-dimensional SbAs semiconductors can also be anticipated to have many other functionalities.

II. CALCULATION METHODS

The total energies and relaxed geometries were calculated by the density functional theory within the generalized gradient approximation [15,16], periodic boundary conditions, and a plane-wave basis set as implemented in the Vienna *ab initio* simulation package [17]. The Perdew-Burke-Ernzerhof exchange correlation functional with projector augmented wave potentials is used in all energy calculations [18]. The total energies were numerically converged to approximately 3 meV/atom with spin-orbit coupling using a basis set energy cutoff of 400 eV and dense k meshes corresponding to 3000 per reciprocal atom k point in the Brillouin zone. A vacuum layer thicker than 10 Å was added for 2D structures to avoid interaction between adjacent periodic images. To describe the van der Waals (vdW) interaction, a correction by the van der Waals density functional method was adopted [19]. The formation energy ΔH of $A_{1-x}B_x$ with respect to the energies of constituents A and B is defined as $\Delta H(\sigma) = E_{\text{tot}}(\sigma) - (1-x)E_{\text{tot}}^A - xE_{\text{tot}}^B$, where $E_{\text{tot}}(\sigma)$, E_{tot}^A and E_{tot}^B are total energies of phases $A_{1-x}B_x$, A and B , respectively.

To calculate the band gap for a given unit cell, the energy eigenvalues at each k point in the Brillouin zone are evaluated and the band-gap values are determined from the difference between the conduction-band minimum (CBM) and valence-band maximum (VBM). The cluster expansion approach [20] was used to construct an effective Hamiltonian for energy evaluation on rhombohedral structures. We used the ATAT toolkit [21] to obtain the optimal effective cluster interactions from fully relaxed total energies of ordered input structures. By fitting 30 ordered input structures, the final cluster expansion uses 13 effective cluster interaction coefficients,

including 11 pair interactions, resulting in a leave-one-out cross-validation score of as good as 3 meV/f.u.

Based on the converged effective cluster interactions, the temperature-composition phase diagrams are calculated by semi-grand canonical Monte Carlo simulations [22]. In this semi-grand canonical ensemble, the energy and concentration of an alloy (with a fixed total number of atoms) are allowed to fluctuate while temperature and chemical potentials are externally imposed. By scanning over temperature and chemical potentials, the two-phase regions in the phase diagram can be determined from discontinuities of composition as a function of chemical potential. We use a $40 \times 40 \times 40$ unit cell as a simulation cell, and the simulated temperatures range from 25 to 1000 K with a 25 K interval. We use 40 000 MC steps to equilibrate and 100 000 MC steps for averaging, and we monitor the composition change with the chemical potential at a given temperature. The thermodynamic state is thus determined as a function of the temperature and the chemical potential differences of the constituents. To check for hysteresis in the phase diagram results, we have repeated Monte Carlo simulations by stepping through the chemical potential in both directions. We find no big differences between these two simulations, confirming the accuracy of the phase diagrams.

III. THERMODYNAMIC PROPERTIES

Using the DFT+CE computational methodology, we predict the stable phases of $\text{Sb}_x\text{As}_{1-x}$ and the formation energy of all 61 959 As-type ordered structures with fewer than 14 atoms per unit cell shown in Fig. 1(a). By constructing the convex hull (the lowest-energy set of tie lines such that no structure lies below the hull), we can identify the ground state structures at 0 K as a function of composition. Figure 1(a) shows that the formation energies of the $\text{Sb}_x\text{As}_{1-x}$ structures are often positive, but some configurations are negative, indicating stability of the compounds relative to the pure end members As and Sb. Even though As and Sb are in the same prototype rhombohedral structure, the relative large lattice mismatch ($>7.4\%$) induces a relatively strong strain energy penalty, which directly induces positive formation energies. Sb-As nevertheless forms a stable ordered compound SbAs with negative formation energy relative to As and Sb. To explain the trend of forming Sb-As atom pairs in ordered structure, we plot the pair interaction J_{pair} as a function of pair distance for $\text{Sb}_x\text{As}_{1-x}$ in Fig. 1(c). It can be seen that short-range pairs J_{pair} for the nearest and next nearest neighbor pairs are both positive with much larger magnitude than long-range negative interactions. The positive pair interactions lead to repulsion between atoms with the same species, thus indicating clustering of like bonds As-As or Sb-Sb is prevented and Sb-As ordered bonds are favorable.

Using the DFT-derived cluster expansion, we determine the temperature-composition phase diagram of Sb-As by GCMC simulations [Fig. 1(b)]. There is one predicted ordered phases in the phase diagram, corresponding to one $T = 0$ K ground state with SbAs stoichiometry. We note, however, that at finite temperatures, the phase is stable for a range of off-stoichiometric compositions. Also, the phase undergoes an order-disorder transformation into a stable, disordered

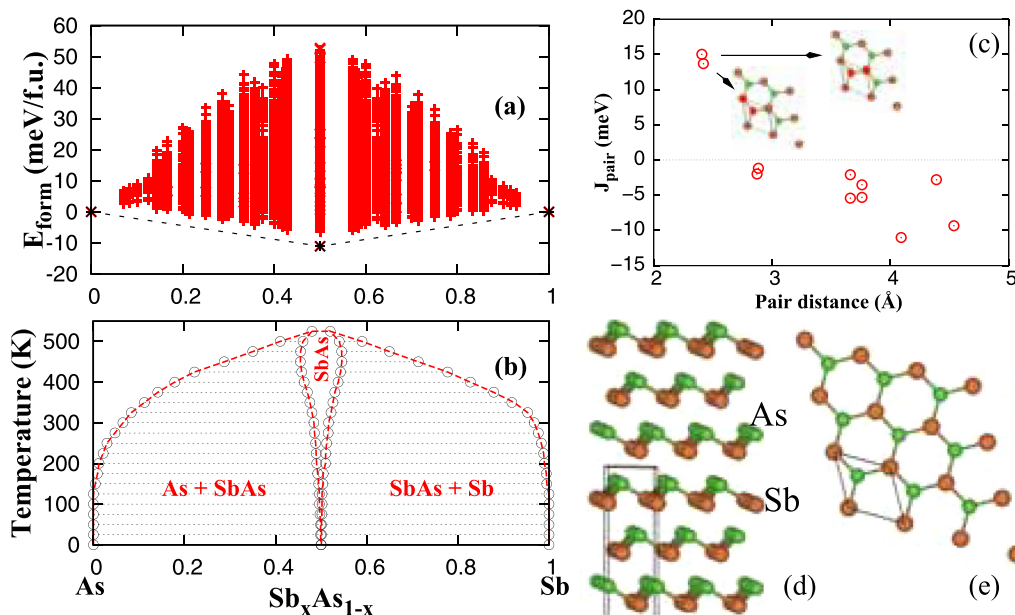


FIG. 1. Formation energy (a) and temperature-composition phase diagram (b) of As and Sb alloying phases. The plus sign means the energies predicted by cluster expansion for possible structures; the star sign indicates the energies of DFT calculated ground states. The pair interaction as a function of pair atom distance is plotted in (c). The nearest and next nearest pair interaction configuration are shown in red in inset figures in (c). The ordered phase is SbAs, corresponding to the ground states at 50% in (a). The crystal structure of ordered SbAs is plotted in (d) with a layer of atoms in top view shown in (e).

rhombohedral solid solution at 525 K. There are also two regions of stable two-phase coexistence. The calculated phase stability agrees well with previous results [23].

A side view of calculated SbAs structure and a top view of one-layer SbAs are, respectively, shown in Figs. 1(d) and 1(e). It is clear that SbAs is in a layered polar structure (space group $R-3m$) with van der Waals gap in the z direction, which is the same as the prototype As structure. In each layer of SbAs, As and Sb are ordered forming a buckled honeycomb configuration. The calculated lattice parameters $a = b = 4.11 \text{ \AA}$, $c = 10.94 \text{ \AA}$ agree well with experimental observations of $a = b = 4.066$, $c = 10.889 \text{ \AA}$ [9]. To verify the order-disorder transition temperature of SbAs (525 K), we also performed canonical Monte Carlo simulations at this 50% composition to monitor the energy change as a function of temperature. We found there is an abrupt energy increase at 525 K, suggesting a first-order transition to a disordered phase with a higher energy. The calculated order-disorder transition temperature is also in good agreement with the experimental observation of 550 K [9]. Another important feature of the experimentally synthesized SbAs is that there is 20% antisite disorder in the annealed sample [9]. To verify this information, we also calculate the antisite percentage in SbAs as a function of temperature (shown in Fig. S1 in the Supplemental Material [24]) by canonical Monte Carlo simulations. The percentage of antisite is evaluated by the $P_{\text{anti}} = 100 n_{\text{SbAs}} / 2n_{\text{tot}}$, where n_{SbAs} is the number of Sb atoms occupying As sites, and n_{tot} is the total number of As and Sb sites. The percentage of antisites is related to the large-range order (LRO) parameter of this compound. The number of antisites is averaged from ten snapshot configuration samples at each temperature from Monte Carlo simulations. As we can see, the antisite percentage gradually increases with temperature to about 12%

at 525 K and then significantly increases to $\sim 50\%$ at 550 K (above the order-disorder transition). The maximum antisite percentage is close to experimental observation of 20% antisite, and the abrupt increase of percentage we find in the SbAs phase at the order-disorder transition temperature is consistent with the loss of LRO in the disordered solid solution.

IV. ELECTRONIC BAND STRUCTURE TRANSITION

Having established a stable layered structure of SbAs, we can now examine the variation of the electronic band structure of SbAs upon reducing the number of atomic layers. Here we define one layer as containing atoms of Sb and As in the buckled honeycomb configuration. As shown in Fig. 2(a), bulk SbAs exhibits a semimetallic behavior due to weak overlap of valence and conduction bands at the Fermi level. This semimetallic behavior is similar to the bulk As and Sb [9]. The semimetallic character of bulk SbAs (Fig. 2) is due to the overlap between As $4p_x$ orbital conduction bands at the L point and Sb $5p_x$ orbital valence bands along the B - Z direction. The p_y , p_z orbitals from As and Sb contribute very little to the conduction band minimum and valence band maximum. SbAs preserves the semimetallic character when the bulk compound is thinned down to a trilayer as shown in Fig. 3(d). The semimetallic character of trilayered SbAs is mainly due to the fact that the As $4p_z$ and Sb $5p_z$ orbitals cross the Fermi level at several points in the Brillouin zone.

A significant change occurs in the band structure when the thickness is decreased to a bilayer, and a small band gap of 0.06 eV is observed [Fig. 3(a)]. These results demonstrate that a band gap opens, transforming the SbAs material into a 2D narrow-band-gap semiconductor. The CBM of SbAs mainly consists of As $4p_z$ and Sb $5p_z$ states as shown in the

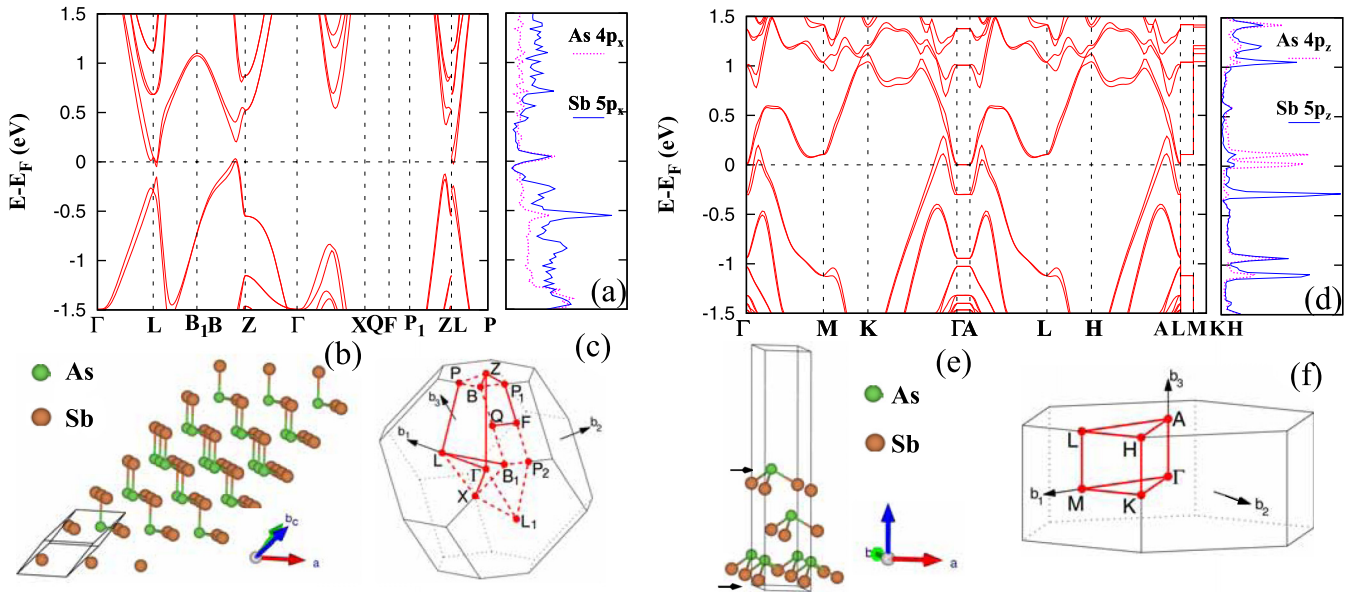


FIG. 2. Electronic band structure and projected DOS of (a) bulk SbAs and (d) trilayer SbAs. The atomic structure of (b) bulk and (e) trilayer SbAs, and corresponding Brillouin zones (c), (f). Note that the bulk SbAs has $R-3m$ space group, which corresponds to the rhombohedral Brillouin zone, while the trilayer SbAs has a $P3m1$ space group corresponding to the hexagonal Brillouin zone [25].

projected density of states (DOS) [Fig. 3(a)] with very minor contributions from As $4p_x$, $4p_y$ and Sb $5p_x$, $5p_y$ states. As shown in Fig. 3(a), the valence band maximum of the SbAs bilayer mainly consists of As $4p_z$ states and Sb $5p_z$ states. However, for monolayer SbAs, the conduction band shifts

up significantly while the valence band shifts down slightly, resulting in a sharp decrease of the valence and conduction band overlap and thus in the formation of a 1.28-eV band gap. Different from the trilayer and bilayer cases, in monolayer SbAs, the valence band maximum has a strong contribution from As $4p_x$, $4p_y$ states [Fig. 3(b)] and Sb $5p_x$, $5p_y$ states (Fig. S2 in the Supplemental Material [24]). The CBM consists of many relatively small contributions from As $4s$, $4p_x$, $4p_y$, $4p_z$ states [Fig. 5(b) inset] and Sb $5s$, $5p_x$, $5p_y$, $5p_z$ states (Fig. S2 inset) [24]. Due to similar contributions of Sb to band structure as those of the As atom, the projected DOS of Sb in the monolayer are shown in Fig. S2 [24]. The couplings between As($4s$) Sb($5s$) and As($4p$) Sb($5p$) split into three bonding and three antibonding states forming a band gap. The VBM is at the Γ point and the CBM along the Γ -M and A-L directions. Therefore, the freestanding SbAs monolayer is an indirect semiconductor with a band gap of 1.28 eV due to the 2D quantum confinement effect. This result is analogous to the previous calculations on As [26,27] and Sb [26] band transitions from multilayer to monolayer. It is also interesting to see that there is not a strong band bowing effect since the calculated ordered monolayer SbAs band gap is 1.28 eV, which is very close to an average of monolayer As (1.58 eV) and monolayer Sb (1.01 eV).

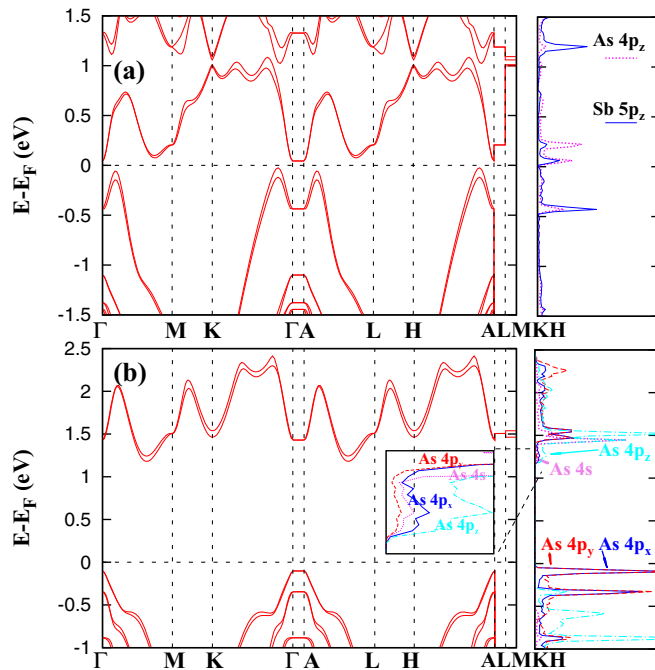


FIG. 3. Band structure and projected DOS of (a) bilayer and (b) monolayer SbAs. In (b), the DOS around the conduction band bottom (1.1–1.4 eV) are enlarged as an inset figure. For the bilayer and monolayer configurations, the Brillouin zone is the same as the trilayer and is shown in Fig. 4(c).

To gain further insights, we also computed isosurfaces of electron density difference defined by $\Delta\rho = \rho_{\text{tot}} - \rho_{\text{up}} - \rho_{\text{dn}}$. Here ρ_{tot} , ρ_{up} , ρ_{dn} are, respectively, total, upper, and lower charge density for the slab. The charge density is defined such that the positive number means charge accumulation and negative charge depletion. As shown in Fig. S3 in the Supplemental Material [24], within the interlayer, the red depletion isosurfaces above As atom (green) and below Sb atoms (dark yellow) are an indication of the As lone pair electrons, the existence of which results in significant puckering and a Peierls distortion. The red charge depletion and blue

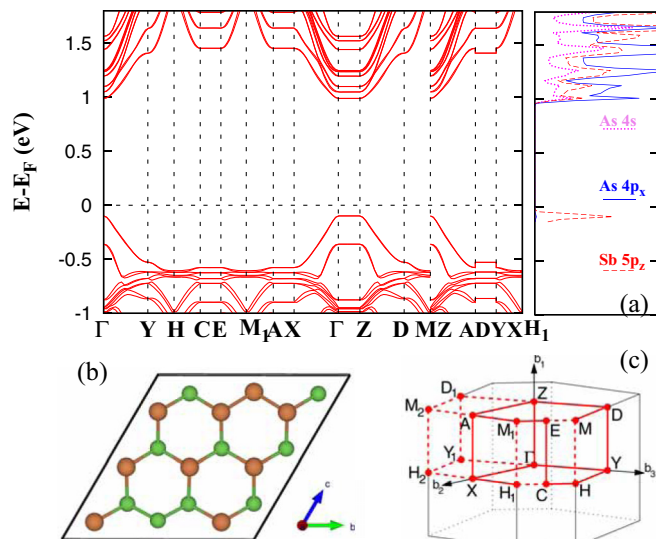


FIG. 4. (a) Band structure and projected DOS of monolayer SbAs with two antisites. The atomic structure of a monolayer with antisites is shown in (b) and corresponding Brillouin zone in (c).

accumulation within the interlayer also reflects a relatively strong bonding between layers (Fig. S3 [24]). We believe that the strong interlayer interaction likely plays an important role in the semimetal-to-semiconductor transition in the SbAs system.

Indirect band-gap semiconductors suffer from poor efficiency of light emission in optoelectronic devices. Thus, indirect-to-direct band-gap transitions are still a very active research field. The monolayer SbAs also experiences an intriguing indirect-to-direct band-gap transition at a relatively small strain. Our calculations indicate that the freestanding SbAs has an indirect band as shown in Fig. 3(b) with VBM at Γ and CBM along Γ - M . However, the band structure of monolayer SbAs with a 1% tensile strain develops a CBM at the Γ point and forms a direct band. However, our phase stability calculations have shown that even strain-free monolayers are unlikely to be defect free, so we consider the band structure of monolayer SbAs with antisites. For monolayer SbAs, we assume that the antisite percentage is similar to that of the bulk case. It is clear from Fig. 4 that freestanding SbAs with antisites has a direct band structure with both VBM and CBM at the Γ point. The CBM of the monolayer antisite is mainly due to the coupling between As(4s), As(4p_x), and Sb(5p_z) as shown in projected DOS in Fig. 4(a). The symmetry of SbAs with antisites is thus changed and a new Brillouin zone adopted [Fig. 4(c)]. The indirect-to-direct band transition in monolayer SbAs is partially due to a tensile strain effect, which is similar to the pure As and Sb cases, since the lattice constant of SbAs with antisites is about 0.5% larger than pure SbAs.

V. EXFOLIATION ENERGY

To quantitatively characterize interlayer interaction of SbAs as a potential guide for experimental monolayer synthesis, we evaluate exfoliation energy as a function of interlayer distance and compare this with two benchmark materials,

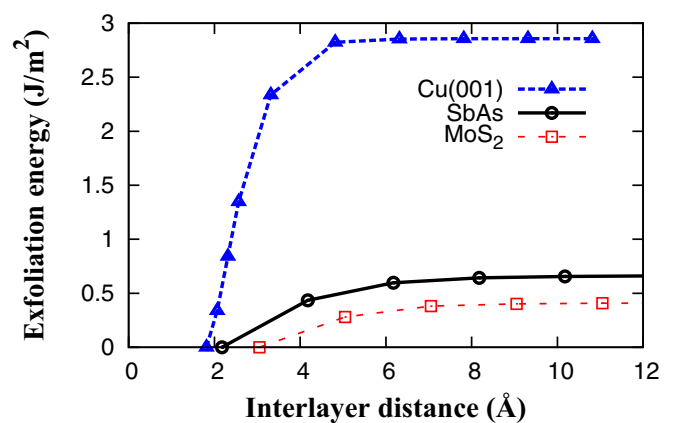


FIG. 5. Exfoliation energy of SbAs as a function of interlayer distance and comparison with MoS₂ and Cu(001). The exfoliation energies of each material are referenced to the corresponding total energies at equilibrium structures. The van der Waals interaction [19] is considered for MoS₂ and SbAs, but not included in Cu(001) calculations.

MoS₂ and Cu(001). The exfoliation energy is calculated by $E_{\text{Ex}} = (E_{\text{Sepa}} - E_{\text{equ}})/A$, where E_{Sepa} is the static total energy of the slab with a layer of SbAs atoms exfoliated relative to the base of the slab, E_{equ} is the total energy of the slab in equilibrium structure, and A is the surface area of the slab. We investigate the exfoliation energy of Cu in the (001) direction just as a point of comparison with a fully 3D metallic structure. As can be seen in Fig. 5, Cu(001) exfoliation energies are about >4.5 times higher than SbAs with an even smaller bond distance (1.86 Å). In comparison with 2D materials, we find the exfoliation energies of SbAs are all higher than MoS₂ at corresponding interlayer distances. The equilibrium interlayer distance of SbAs (2.18 Å) is also much smaller than that of MoS₂ (3.05 Å), suggesting a stronger interlayer interaction than MoS₂. This relative higher exfoliation energy suggests that the mechanical methods for monolayer samples may prove difficult, but chemical deposition methods for monolayer SbAs could be more facile.

VI. SUMMARY

We have constructed the solid state As-Sb phase diagram using a combination of first-principles calculations, cluster expansion, and Monte Carlo simulations. One ordered stable layered structure, SbAs, in the $R-3m$ space group has been found, which agrees very well with previous experimental observations. With well converged effective cluster interactions, Monte Carlo simulations also determined the order-disorder transition temperature of 525 K and the temperature-dependent antisite percentage. Interestingly, the layered SbAs exhibits an electronic band structure transition from bulk semimetallic to monolayer semiconducting behavior due to reduction of strong interlayer interaction and s - p coupling between As(4s) Sb(5s) and As(4p) Sb(5p). Our calculated band structure indicates that the pure SbAs monolayer is an indirect semiconductor with a band gap of 1.28 eV. Moreover, monolayer SbAs undergoes an indirect-to-direct band-gap transition by inclusion of antisite defects, which are present in the

bulk compound for temperature just below the order-disorder transformation. Therefore, this antisite defected monolayer is a potentially very promising system for investigations in nanoelectronic and optoelectronic devices. Moreover, the relatively stronger interlayer interaction of SbAs is characterized by a higher exfoliation energy than MoS₂, implying that chemical deposition methods could be better than mechanical exfoliation methods for monolayer sample preparation.

ACKNOWLEDGMENTS

The authors acknowledge support by the U.S. Department of Energy, Office of Science, Office of Basic Energy Sciences under Award No. DE-SC0014520. We acknowledge the use of the supercomputing resource facilities (Quest) at Northwestern University.

The authors declare no competing financial interest.

-
- [1] D. K. Seo and R. Hoffmann, What determines the structures of the group 15 elements?, *J. Solid State Chem.* **147**, 26 (1999).
- [2] E. Canadell and M.-H. Whangbo, Conceptual aspects of structure-property correlations and electronic instabilities, with applications to low-dimensional transition-metal oxides, *Chem. Rev.* **91**, 965 (1991).
- [3] G. A. Saunders, Semimetals and narrow gap semiconductors, *Contemp. Phys.* **14**, 149 (1973).
- [4] A. Zunger and S. Mahajan, *Handbook on Semiconductors* (North-Holland, Amsterdam, 1992), Vol. 3b.
- [5] S. Hao, L. D. Zhao, C. Q. Chen, V. P. Dravid, M. G. Kanatzidis, and C. M. Wolverton, Theoretical prediction and experimental confirmation of unusual ternary ordered semiconductor compounds Sr-Pb-S system, *J. Am. Chem. Soc.* **136**, 1628 (2014).
- [6] B. J. Skinner, The system arsenic-antimony, *Econ. Geol.* **60**, 228 (1965).
- [7] G. P. Bernardini, C. Cipriani, F. Corsini, G. G. T. Guarini, G. Mazzetti, and L. Poggi, Natural As-Sb alloys: Texture types, thermal behaviour and mechanism of formation, *Mineral Mag.* **51**, 295 (1987).
- [8] H. Ohyama, Thermal conductivity in antimony-arsenic system, *J. Phys. Soc. Jpn.* **23**, 522 (1967).
- [9] D. P. Shoemaker, T. C. Chasapis, D. Do, M. C. Francisco, D. Y. Chung, S. D. Mahanti, A. Llobet, and M. G. Kanatzidis, Chemical ordering rather than random alloying in SbAs, *Phys. Rev. B* **87**, 094201 (2013).
- [10] Q. H. Wang, K. Kalanter-Zaseh, A. Kis, J. N. Coleman, and M. S. Strano, Electronics and optoelectronics of two-dimensional transition metal dichalcogenides, *Nat. Nanotechnol.* **7**, 699 (2012).
- [11] H. Wang, H. Yuan, S. S. Hong, Y. Li, and Y. Cui, Physical and chemical tuning of two-dimensional transition metal dichalcogenides, *Chem. Soc. Rev.* **44**, 2664 (2015).
- [12] T. S. Li and G. Galli, Electronic properties of MoS₂ nanoparticles, *J. Phys. Chem. C* **111**, 16192 (2007).
- [13] S. Lebegue and O. Eriksson, Electronic structure of two-dimensional crystals from *ab initio* theory, *Phys. Rev. B* **79**, 115409 (2009).
- [14] A. Splendiani, L. Sun, Y. Zhang, T. Li, J. Kim, C.-Y. Chim, G. Galli, and F. Wang, Emerging photoluminescence in monolayer MoS₂, *Nano Lett.* **10**, 1271 (2010).
- [15] D. M. Ceperley and B. J. Alder, Ground State of the Electron Gas by a Stochastic Method, *Phys. Rev. Lett.* **45**, 566 (1980).
- [16] J. P. Perdew, J. A. Chevary, S. H. Vosko, K. A. Jackson, M. R. Pederson, D. J. Singh, and C. Fiolhais, Atoms, molecules, solids, and surfaces: Applications of the generalized gradient approximation for exchange and correlation, *Phys. Rev. B* **46**, 6671 (1992).
- [17] G. Kresse and J. Furthmüller, Efficient iterative schemes for *ab initio* total-energy calculations using a plane-wave basis set, *Phys. Rev. B* **54**, 11169 (1996).
- [18] J. P. Perdew, K. Burke, and M. Ernzerhof, Generalized Gradient Approximation Made Simple, *Phys. Rev. Lett.* **77**, 3865 (1996).
- [19] J. Klimeš, D. R. Bowler, and A. Michaelides, Van der Waals density functionals applied to solids, *Phys. Rev. B* **83**, 195131 (2011).
- [20] J. M. Sanchez, F. Ducastelle, and G. Gratias, *Physica A (Amsterdam, Neth.)* **128**, 334 (1984).
- [21] A. van de Walle, M. Asta, and G. Ceder, The alloy-theoretic automated toolkit: A user guide, *CALPHAD: Comput. Coupling Phase Diagrams Thermochem.* **26**, 539 (2002).
- [22] A. van de Walle and M. Asta, Self-driven lattice-model Monte Carlo simulations of alloy thermodynamic properties and phase diagrams, *Modell. Simul. Mater. Sci. Eng.* **10**, 521 (2002).
- [23] A. Ektarawong, Y. P. Feng, and B. BALLing, Phase stability of three-dimensional bulk and two-dimensional monolayer As_{1-x}Sb_x solid solutions from first principles, *J. Phys.: Condens. Matter.* **31**, 245702 (2019).
- [24] See Supplemental Material at <http://link.aps.org/supplemental/10.1103/PhysRevMaterials.3.106002> for calculated antisite percentage in SbAs, bandstructure, and charge density of monolayer SbAs.
- [25] S. Curtarolo, W. Setyawan, G. L. W. Hart, M. Jahnatek, R. V. Chepulskii, R. H. Taylor, S. Wang, J. Xue, K. Yang, O. Levy, M. Mehl, H. T. Stokes, D. O. Demchenko, and D. Morgan, AFLOW: An automatic framework for high-throughput materials discovery, *Comput. Mater. Sci.* **58**, 218 (2012).
- [26] S. Zhang, Z. Yan, Y. Li, Z. Chen, and H. Zeng, Atomically thin arsenene and antimonene: Semimetal-semiconductor and indirect-direct band-gap transitions, *Angew. Chem., Int. Ed.* **54**, 3112 (2015).
- [27] L. Kou, Y. Ma, X. Tan, T. Frauenheim, A. Du, and S. Smith, Structural and electronic properties of layered arsenic and antimony arsenide, *J. Phys. Chem. C* **119**, 6918 (2015).